Essential Chem

ISSN: 2837-8083 (Online) Journal homepage: www.tandfonline.com/journals/tess20

Targeting TACE in breast cancer: exploring the therapeutic potential of cinnoline derivatives through computational and experimental approaches

Chidambaram Mylam Sreenivasan , Panneerselvam Theivendren & Saravanan Govindaraj

To cite this article: Chidambaram Mylam Sreenivasan , Panneerselvam Theivendren & Saravanan Govindaraj (2025) Targeting TACE in breast cancer: exploring the therapeutic potential of cinnoline derivatives through computational and experimental approaches, Essential Chem, 2:1, 2536553, DOI: 10.1080/28378083.2025.2536553

To link to this article: https://doi.org/10.1080/28378083.2025.2536553

Published online: 25 Jul 2025.

ESSENTIAL CHEM
2025, VOL. 2, NO. 1, 2536553
https://doi.org/10.1080/28378083.2025.2536553

Taylor & Francis
Taylor & Francis Group

Targeting TACE in breast cancer: exploring the therapeutic potential of cinnoline derivatives through computational and experimental approaches

Chidambaram Mylam Sreenivasan, Panneerselvam Theivendren, and Saravanan Govindaraj

Department of Pharmaceutical Chemistry & Analysis, School of Pharmaceutical Sciences, Vels Institute of Science, Technology & Advanced Studies, Chennai, India

ABSTRACT

Women throughout the world experience breast cancer as the leading type of malignancy and their numbers continue to increase as mortality numbers remain high especially throughout developing nations. Breast cancer progression depends heavily on TACE/ADAM17 to activate epidermal growth factor receptor (EGFR) thus promoting tumor expansion and metastatic activity. Medical researchers have identified TACE inhibition as an effective way to control tumor expansion and bypass drug obstacles. Cinnoline represents a nitrogen-containing heterocyclic compound that shows significant anticancer activity thus qualifying as a promising target therapy agent. This research investigates the therapeutic value of cinnoline derivatives for TACE inhibitor treatment in breast cancer patients using computational methods and laboratory experiments. Scientists produced novel compounds of 3-acetyl-6-(substituted benzoyl) cinnolin-4(1 H)-one C10 derivatives through characterizations which included FTIR, NMR, and mass spectrometry analysis. The evaluation of TACE binding potential used both molecular docking techniques and molecular dynamics simulations. A MTT cytotoxicity assay performed on MCF-7 breast cancer cells helped examine the anticancer properties. The pharmacokinetic characteristics together with drug-likeness assessment of compounds were determined through ADMET predictions. The study shows promising potential of cinnoline derivatives to function as future potent drug candidates for breast cancer treatment that specifically targets TACE. Ongoing research with cinnoline derivatives will need to test their therapeutic efficacy as well as determine optimal pharmaceutical characteristics for medical use.

ARTICLE HISTORY
Received March 26, 2025
Accepted July 15, 2025

KEYWORDS
Breast cancer; cinnoline derivatives; cytotoxicity; drug discovery; molecular docking; TACE inhibitors

1. Introduction

Women worldwide develop breast cancer at the highest rate and this cancer type creates substantial healthcare resource challenges. Statistically breast cancer generates annual worldwide incidence of 2.3 million new cases which constitute a global cancer diagnosis share of 11.7% reports the World Health Organization (WHO). [1,2] The United States and European countries together with other high-income regions benefit from sophisticated screening systems as well as enhanced treatment procedures which result in better patient survival. [3,4] Patients in developed nations that undergo screening and targeted treatment access survive their cancer for five years at rates above 85%. Treatment access and patient result variables differ across populations because of racial background and social status variations as to these play a role in obtaining healthcare services. The countries of India and various nations in Africa with developing economies encounter difficulties in breast cancer management because of delayed diagnosis and insufficient healthcare centers alongside financial obstacles. [5,6] The percentage of breast cancer cases among females in India comprises 25-32% of all breast cancers while new cases are projected to reach 178,000 per year annually. Breast cancer patients in Western countries survive better than those from Southern Asian regions because more than half of their cases are identified during late stages of development. The combination of insufficient healthcare services and cultural traditions and low patient knowledge about breast cancer

CONTACT Saravanan Govindaraj sarachem1981@gmail.com Department of Pharmaceutical Chemistry & Analysis, School of Pharmaceutical Sciences, Vels Institute of Science, Technology & Advanced Studies, Pallavaram, Chennai, 600117, India

in sub-Saharan Africa leads to delayed medical care which raises mortality statistics. [7,8] Global initiatives including the WHO Global Breast Cancer Initiative work together with Indian national programming through the National Cancer Control Programme (NCCP) to improve breast cancer detection while enhancing treatment accessibility while promoting cancer research. Breast cancer management is undergoing radical change because of fresh treatment strategies which use molecular-targeted approaches along with personalized medicine therapy. The progression of breast cancer depends heavily on Tumor necrosis factor-alpha-converting enzyme (TACE/ADAM17) because it enables cellular signaling pathways that control tumor growth and enables metastasis. [9,10] The cancer-related protein epidermal growth factor receptor (EGFR) ligands with other proteins experience shedding through TACE-mediated mechanisms. Clinical data shows that excessive TACE expression in breast cancer tissues connects to elevated tumor invasiveness as well as detrimental treatment outcomes and anticancer drug resistance. [11,12] New research confirms that TACE inhibitor medications successfully minimize tumor size and strengthen the effectiveness of chemotherapy drugs. The blocking of TACE-mediated EGFR signaling shows promise as an attractive breast cancer therapy by suppressing angiogenesis together with resistance mechanisms and tumor invasion. Medical experts believe that adding TACE inhibitors to combination treatment protocols shows potential as a method for achieving better results in treatments for aggressive breast cancer types. [13,14] The heterocyclic compound Cinnoline containing nitrogen attracts researchers in drug development because of its broad clinical scope which includes anti-inflammatory effects and antimicrobial effects and anticancer activities. Breast cancer research shows that cinnoline derivatives unite powerfully with cancer-related molecular targets thus blocking essential cell cycle control mechanisms and apoptosis pathways and signal transduction functions. Researchers have proven through computational and experimental methods that cinnoline derivatives show high cytotoxic potential toward breast cancer cell lines. [15–17] TACE enzyme inhibition coupled with disrupted EGFR signaling mechanisms makes these compounds promising drug candidates for managing drug-resistant breast cancer cells. Scientists can achieve better bioactivity and selectivity and lower toxicity levels through designing novel analogs based on cinnoline structure. The research evaluates cinnoline derivatives as potential cancer fighting compounds for breast cancer management through their effects on TACE (ADAM17) molecular targets. [18] The combination of experimental methodology with computational analysis through this research initiative will lead to the development of strong TACE blocking cinnoline inhibitors for implementing effective breast cancer therapies.

2. Materials and methods

2.1. Materials

All available reagents and starting materials and solvents used for synthesis were obtained either from commercial vendors or from grade analytical standards. Workers used open capillary tubes to determine melting points so they needed to apply corrections for the results. KBr pellets operated the ABB Bomem FT-IR spectrometer MB 104 produced by ABB Limited located in Bengaluru, India, to record IR spectra. The Proton nuclear magnetic resonance (1 H NMR) spectra ran on a Bruker 400 NMR spectrometer from Mumbai, India, through the use of tetramethylsilane as internal reference. Elemental analysis micro-measurements used a V300 Vario EL from Analysensysteme GmbH while mass spectral acquisition happened with a Shimadzu GC MS QP 5000 quadrupole mass spectrometer provided by Chennai, India. The chemical purity checks employed thin-layer chromatography using SiO_2 gel plates with 200 mesh size from E. Merck as the supplier. The obtained elemental results along with IR spectroscopy and both proton ^{1}H and carbon-^{13}NMR together with mass spectrometry data supported the identified molecular structures.

2.2. Molecular target prediction

Active breast cancer components identified their targets using Genecards and OMIM Swiss target prediction and Gprofiler and ShinyGO along with Venn diagrams. A set of Venn diagrams demonstrates target information through visual representations of overlapping circular sections.

Visual comparisons between groups of breast cancer-linked components or variables become feasible through this method. Breast cancer risk factors are displayed by circles that overlap within the diagrams for each cancer type. [19]

2.3. Statistics of the Ramachandran plot

Users can find extensive summaries of Protein Data Bank (PDB) entry structural data through the PDBsum web server located at https://www.ebi.ac.uk/thorntonsrv/databases/pdbsum/. The system provides complete dataset access about Ramachandran plot statistics through the combination of PDB ID entries or file uploads containing structural data. Apart from its functional attributes the server produces graphical output of secondary structure elements alongside protein-ligand and protein-protein interaction displays. The system combines structural evolutions with enzyme active sites and mutation effects to provide all needed information. The structural biology community and bioinformatics specialists depend on PDBsum as a critical platform for accessing three-dimensional information about biomolecule structures and their connections while obtaining functional data. [20,21]

2.4. Protein preparation

We retrieved protein structural information from the Protein Data Bank (PDB) through its website https://www.rcsb.org/ that falls under management of the Research Collaboratory for Structural Bioinformatics (RCSB). A protein stored within the database utilizes the identifier 3WEJ (TACE) for specific identification. The CHARMM-GUI program processed all proteins through pre-analysis steps that included the removal of absent residues and the elimination of unneeded water molecules and ligands. [22–24]

2.5. Ligand preparation

Breast cancer research determined that twenty-five compounds categorized as 3-acetyl-6-(substituted benzoyl)cinnolin-4(1H)-one demonstrated potential anti-breast cancer properties when evaluated along with their cocrystals which include 3WEJ (TACE). The ".sdp" data files for these compounds originated from the free-access PubChem database located at (https://pubchem.ncbi.nlm.nih.gov/). By using BIOVIA Discovery Studio Visualizer tool users can prepare cluster analysis of each compound and cocrystal through https://discover.3ds.com/discovery-studio-visualizer-download. [22–24]

2.6. Molecular docking protocol

AutoDock Vina-POAP performed intermediate tasks which included converting both proteins and ligands to pdbqt file formats. The configuration file stored information about the protein and ligand in addition to grid box dimension parameters. The application process added polar hydrogens and solvation parameters together with fragmental volumes to the protein. The AutoGrid application built the grid map box that existed between three specified coordinates for x, y, and z dimensions. The established ligand structure served as the basis to develop a scoring grid which increased operational speed during computation. The docking process that AutoDock Vina conducts for proteins and ligands depends on iterated local search optimization to find global solutions based on the assumption of unchanging structural components. The results exhibiting minimum free energy as binding metric were obtained after removing all outcomes that exceeded 1.0A positional root mean square deviation. The final docking position for analysis of amino acid cooperations was selected from those poses showing minimal binding potential through BIOVIA Discovery Studio Visualizer analysis. Proteins must have molecular attachment areas for binding purposes which support chemical reactions and generate proper residual sites for bioactive molecules. The binding of proteins and enzymes with their target enzymes depends on precise sites located within the molecules. The PrankWeb system (https://prankweb.cz/) successfully located every active site among the target chemicals. The last step produced a receptor grid for the protein active site through AutoDock Vina-POAP virtual screening. [22–25]

2.7. Molecular dynamics protocol

The molecular simulations focused on examining drug substances as well as their attachment patterns to protein receptors for interaction stability evaluation. The Desmond module operated from Linux-based Maestro simulation platform by Schrödinger Inc. to perform the simulations. Using TIP3 water boundaries the system required Na+ and Cl-salts to achieve proper 0.15 M concentration balance. The simulations conducted through NPT ensemble kept the platform at 300 K while utilizing 1.01325 bar pressure. Scientists examined TACE protein (3WEJ) while binding with 3-acetyl-6-(4-nitrobenzoyl)cinnolin-4(1H)-one (C10) for 100 nanoseconds during the research. Processing of simulation results with Desmond involved the use of simulation interaction diagrams for advanced analytical purposes. The assessment of stability consisted of RMSD and RMSF measurements together with protein-ligand interaction examination. [22–24]

2.8. Density functionality theory

The referenced compounds include 3-acetyl-6-(4-nitrobenzoyl)cinnolin-4(1H)-one (C10). Public data files of substances were acquired from the PubChem public depository in the form of.SDP files. Spartan14 graphical interface served to conduct energy minimization operations on the files. The software GaussView 6.0.16 enabled the calculation of HOMO and LUMO orbital Hartree energies. Scientists required electron-voltage measurements from Hartree energy values to conduct stability assessments on C10 molecular stability. [22–24]

2.9. ADMET modeling

In silico ADME assessments together with ADME studies, distribution and excretion studies with physicochemical property assessments established the effectiveness and stability of compound C10. The SwissADME web service (http://www.swissadme.ch/) conducted assessment on molecular weight, molar refractivity, solubility together with bioavailability and additional elements that included radar maps and the egg-boiled model and brain penetration and human gastrointestinal absorption. The no-cost web service SwissADME permits scientists to forecast the pharmacokinetic properties along with drug-likeness characteristics for their test compounds and reference substances. [22–24]

2.10. Synthesis

A 10 mL solution of 4-chloroaniline first reacted with ethyl acetoacetate solution before receiving 7 mL NaNO2 solution while continuously cooling to result in dilute HCl (10% w/w, 200 ml) introduction into the mixture. Refining the mixture with water bath heating produced a solid substance which was filtered and cleaned with 5% NaOH solution followed by water to obtain compound 3-(2-(4-chlorophenyl)hydrazineylidene)hexane-2,4-dione 1I. Solution of Compound 1I (13 mmol) in chlorobenzene (30 ml consumed anhydrous AlCl3 powder (37 mmol) simultaneously with the mixture kept at low temperature. A heated liquid reaction took place by performing the reflux under anhydrous conditions during sixteen hours. The solution needed cooling temperatures before it underwent treatment with 200 ml of 10% w/w dilute HCl. The mixture required a water bath heat to purify its chlorobenzene before distillation occurred through steam. Washing the obtained solid with successive solutions of 5% NaOH and then distilled water produced the final product 3-acetyl-6-chlorocinnolin-4(1H)-one 2I. The process to dissolve compound 2I involved adding 7 mL of 96% ethanol to it for dissolving followed by the addition of a single equivalent of substituted benzaldehyde. One equivalent of substituted benzaldehyde solution was added through micro pipetting to the split portion of the solution. The solution stirred within the apparatus during three hours of reflux operation. The solution was adjusted to +4oC while stored under room temperature conditions for twelve hours. After filtration and drying as well as water washing of the reaction mixture the 3-acetyl-6-(substituted benzoyl) cinnolin-4(1H)-one derivatives Scheme 1 appeared as final crystallized products.

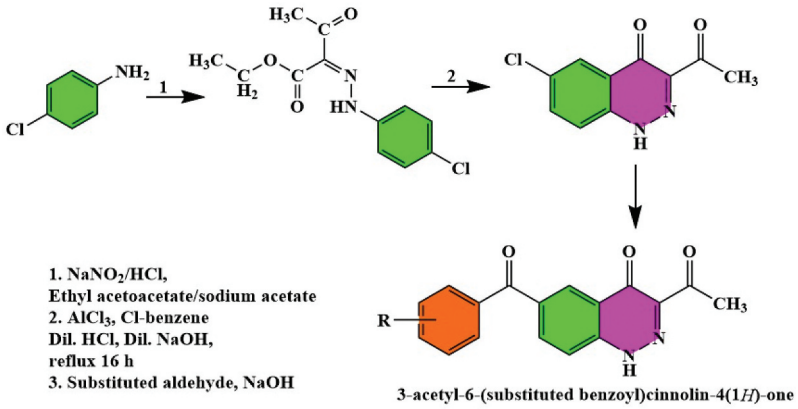

2.11. MTT assay

The MCF-7 cell line which NCCS obtained grew in DMEM medium supplemented with deactivated 10% FBS along with 100 IU/mL penicillin and 100 µg/mL streptomycin under 5% CO_2 at 37°C and a controlled humidity environment until reaching confluency. The researchers trypsinized cells from the confluent monolayer before adjusting the cell density to 1.0 x 10^5 cells/mL by using medium with 10% FBS. The microtitter plate received 100 µL of cell suspension containing 1 x 10^4 cells/well. The cells received one wash using medium after reaching their partial monolayer state during the 24-hour period. The plate received different concentrations of test samples by adding 100 µL per well into each well before subjecting it to a 37°C incubation period of 24 hours under a 5% CO2 atmosphere. The experiment continued with removal of the test solutions which was followed by adding 20 microliters MTT solution (2 mg/mL MTT in PBS) to each well. A four-hour incubation time under precisely the same temperature and CO2 atmosphere was applied to the plate. DMSO solution received an addition of 100 µL while removing the supernatant from the plate after incubation. A gentle agitation of the plate helped to solve the formed formazan crystals. The microplate reader measured cell viability by detecting absorbance at 570 nm wavelength. The measurement of viability percentage depended on the formula: % viability = (Sample abs/Control abs x 100). [5]

3. Results and discussion

3.1. Molecular target prediction

Researchers evaluated the cinnoline derivative containing a nitrobenzoyl group as a query molecule to determine its suitable target protein families. Several types of biological targets tend to interact with this chemical substance due to its extensive range of pharmaceutical capabilities. [25, The total predictions indicate enzymes as targets comprise 26.7% of the data because this substance modifies biological catalysts necessary for metabolic regulation. The estimated targets composed 20% of Lyases which indicates this molecule might regulate metabolism since Lyases function as enzymes for breaking chemical bonds. The signal transduction process uses this molecule to modify 20% of targeted proteins that are kinases. The drug affects two main groups in the human body: Family A G protein-coupled receptors (6.7%) and cytochrome P450 enzymes (6.7%) together with other significant enzyme categories Figure 1. The molecule demonstrates potential as a polypharmacological agent since its broad response targets make it an attractive prospect for therapeutic approaches targeting multiple targets. Further study is needed to determine the chemical interaction between the molecule and both kinases and cytochrome P450 enzymes when evaluating its potential use in cancer and metabolic disease treatment. Experimental laboratory testing of enzymes and binding receptors alongside testing off-target consequences will serve to confirm the predictions while ensuring both safety and treatment effectiveness.

The Venn diagram depicts 3-acetyl-6-(substituted benzoyl)cinnolin-4(1H)-one derivatives binding with 102 molecular targets yet showing interaction with 18,389 cancer-related targets. Studies identified TACE (ADAM17) as the main common target from a list of 32 targeted proteins which demonstrates strong

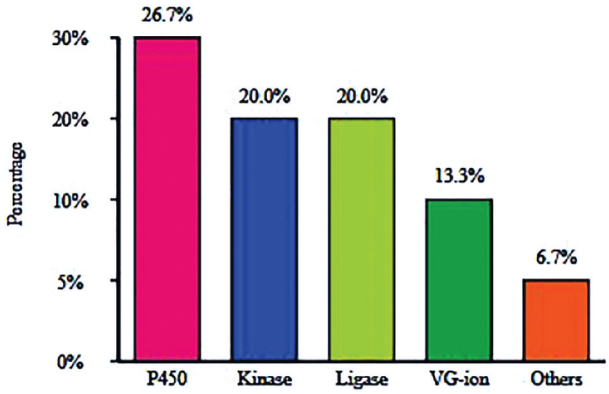

Figure 1. Target prediction of the query molecule: Distribution of top 15 target classes, highlighting significant interactions with enzymes (26.7%), lyases (20%), kinases (20%), and minor contributions from other protein categories.

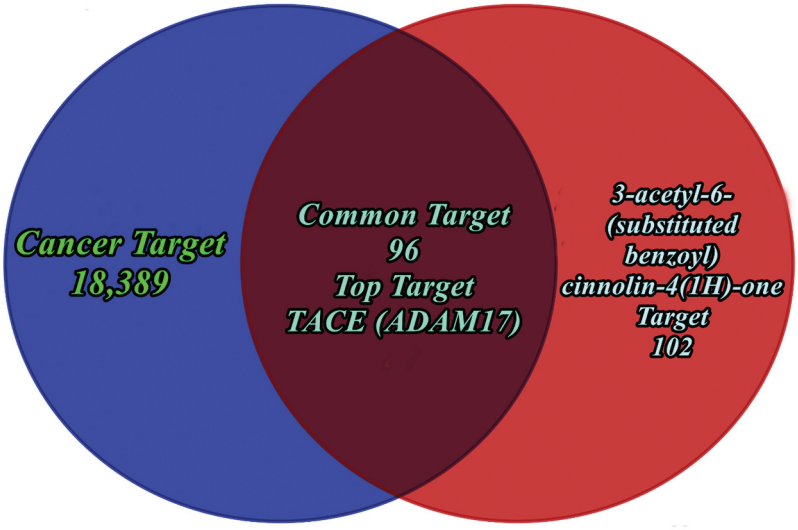

Figure 2. Venn diagram showing the overlap between cancer-related targets (18,389) and 3-acetyl-6-(substituted benzoyl) cinnolin-4(1H)-one targets (102), identifying 96 common targets, with TACE (ADAM17) as the top molecular target for breast cancer inhibition.

alignment between cinnoline derivatives and breast cancer pathways. Laboratory tests demonstrated strong binding capabilities of TACE-related inhibitors with cinnoline derivatives thus reinforcing therapeutic potential. The results support the concept that blocking EGFR signaling through TACE inhibition leads to breast cancer suppression. Experimental tests of cell toxicity succeeded in confirming antitumor effects which demonstrated promising potential for cinnoline derivatives in breast cancer targeted treatment options Figure 2.

3.2. TACE gene network analysis

The analysis demonstrates TACE (ADAM17) functions as an essential network node through numerous connections involving cancer-related and inflammatory along with cell-signaling proteins. Membrane-bound cytokines such as TNF-α undergo proteolytic cleavage through TACE activity which establishes it as a fundamental control element of tumor microenvironments. The proteins EGFR together with PIK3CA and MTOR represent primary genes responsible for driving oncogenic signaling networks. The network of gene and protein relationships suggests TACE generates an indirect impact on cell proliferation and survival and angiogenesis mechanisms thus reinforcing its role in cancer development. Highlights of the central role

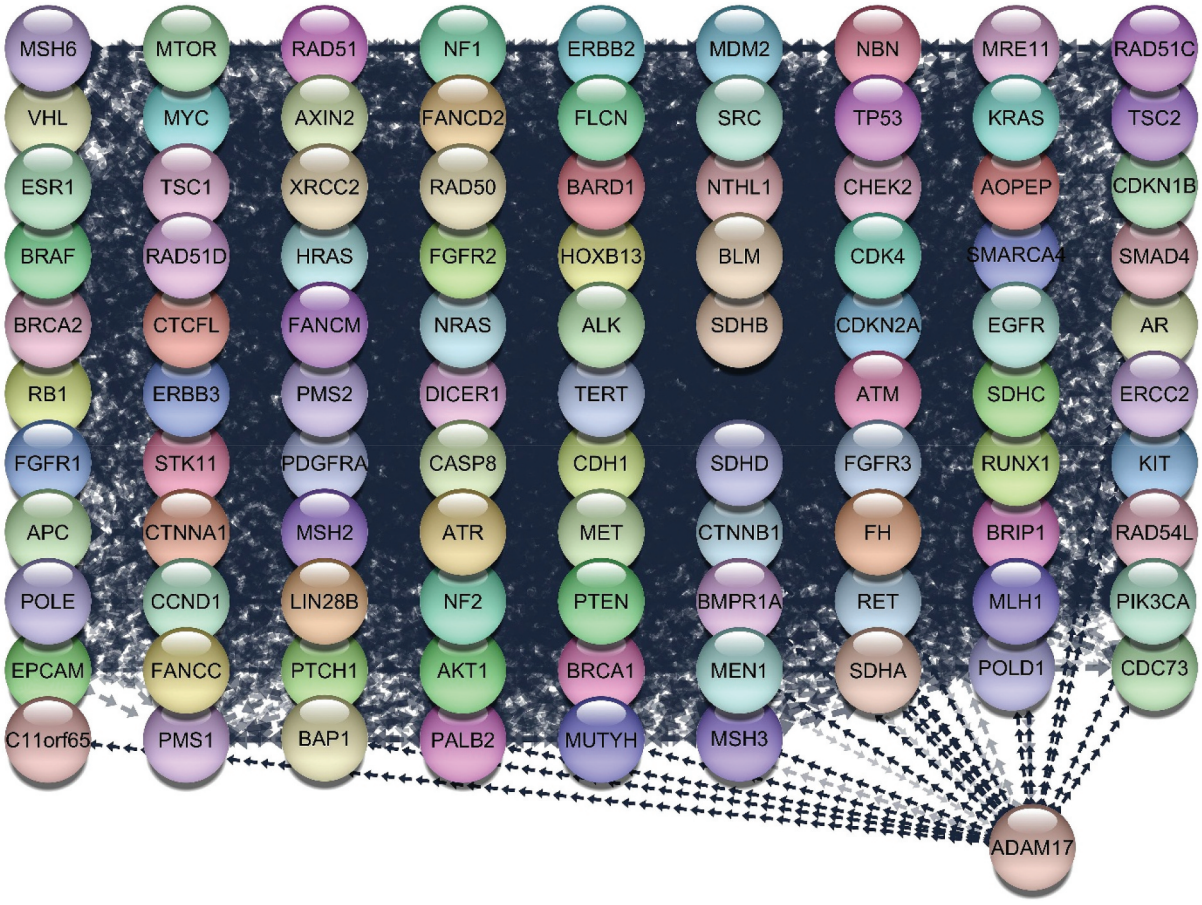

Figure 3. TACE-associated gene network: Visualization of interacting genes and proteins, including TACE (ADAM17), highlighting its central role in signaling pathways relevant to cancer progression, inflammation, and cellular communication.

of TACE in signaling pathways relevant to cancer progression, inflammation, and cellular communication are depicted in Figure 3.

TACE controls tumor development in two ways through its binding activities with the NF1 and PTEN tumor suppressors which enable the regulation of both pathological growth and immune responses. BRAF and KRAS mutation patterns establish TACE as a key participant in cancer cell operations. Tumor cell survival mechanisms show importance because BRCA1/2 and TP53 as DNA repair and apoptosis regulators interact with TACE. The extensive involvement of TACE across different interactions makes it a compelling target platform for cancer treatment. Research showcases how treatment methods combining TACE disruption with inhibition of important proteins such as EGFR or MTOR would enhance therapeutic effects. The inhibition of the TACE enzyme would block its ability to activate TNF-α which would subsequently decrease tumor progression and inflammatory response. This analysis demonstrates that TACE functions as a central node which connects vital oncogenic and inflammatory pathways which supports additional investigations into TACE inhibitor use together with specific pathway pharmaceuticals for increased therapeutic activity.

3.3. TACE mechanism

TACE (ADAM17) functions as a metalloproteinase that completes protease activities on membrane-anchored precursors to release functional cytokine growth factors and various other molecules Figure 4. The enzyme controls vital signaling pathways which control both inflammatory reactions and immune responses together with cancer cell advancement. The activity of TACE breaks down pro-TNF-α into soluble form which enables this cytokine to attach to TNF receptors as it progresses through pathways that

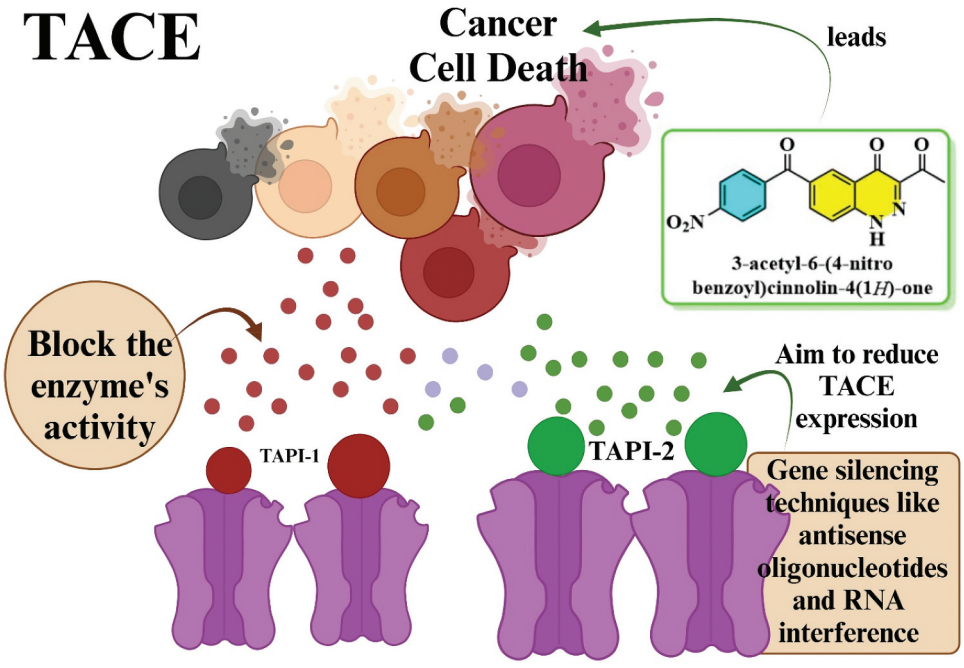

Figure 4. Mechanism of TACE inhibition: Blocking enzymatic activity with inhibitors (TAPI-1, TAPI-2) and reducing TACE expression via gene silencing techniques to promote cancer cell death through targeted therapies.

cause tumor effects and inflammation and promotes metastasis. The elevated or abnormal expression levels of TACE lead to cancer development because it supports tumor-promoting factor release contributing to cancer cell growth and new blood vessel formation and immune system avoidance. The anti-TACE compounds TAPI-1 and TAPI-2 have been developed to stop TACE from performing its catalytic function. As a result of this blocking mechanism active TNF-α cannot escape the cell resulting in both reduced inflammation and tumor expansion. Two alternative therapeutic strategies for TACE exist through RNA interference and antisense oligonucleotides which seek to decrease its transcriptional expression. Research has shown that the compound 3-acetyl-6-(4-nitrobenzoyl)cinnolin-4(1H)-one C10 has the ability to function as a TACE inhibitor by hindering its enzymatic activity which results in cancer cell mortality. Research indicates TACE inhibition has therapeutic applications in treating cancer and inflammatory conditions as a single therapeutic approach. Additional studies need to be conducted in order to make these approaches clinically ready.

3.4. Ramachandran plot analysis

The Ramachandran plot analysis shows most non-glycine and non-proline residues occupy areas known as most favored regions (A, B, L) which verifies proper bond torsions in the model. The model shows reliable performance based on its high percentage of preferred region residues which exceeds normal quality requirements. Most residues exist in additional allowed areas and the rest occupy generous stretches of space with a tiny population of residues positioned there. The disallowed regions contain a small proportion of residues potentially because proline shows high rigidity while glycine demonstrates natural flexibility. The G-factor score indicates the model executes its structural functions effectively because atomic position clashes remain minimal. The structural accuracy is confirmed through bond length and angle measurements which match regular values in the main chain. The Phi-Psi angle scores manifest as a marginally negative distribution yet still stay within the accepted ranges. Information about backbone stability arises from positive Chi3 and Chi4 values that show the structure exists in an orderly manner. The secondary structure map shows distinct arrangements of α-helices and β-sheets and turns. The design structure shows good equilibrium between secondary elements and functional sites maintain their expected structural configurations which demonstrates correct placement of fundamental residues at these sites Figure 5.

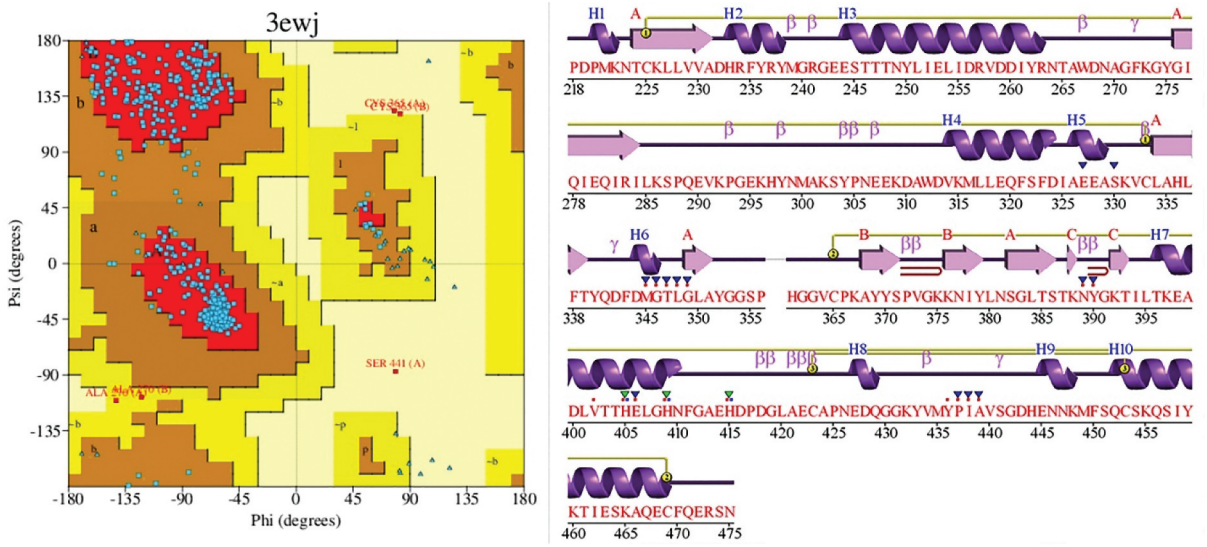

Figure 5. Ramachandran plot and secondary structure analysis of the protein model showing residue distribution in favored regions and structural elements, including α-helices, β-sheets, and potential disallowed conformations.

3.5. Molecular docking analysis

3.5.1. Ligand docking results

The highest binding affinity from docking results landed on C10 (4-NO_2) with −11.4 score while C15 (2-NH_2), C23 (3-Br), and C3 (2-OH) ranked closely behind with −10.9 score each. The high consistency of scoring positions indicates strong active site bond potential for the ligands. The binding interactions of ligands C17 (3-F) and C24 (4-Br) appear to be weakened because their scores amount to −9.8 and −9.7 respectively. The 3EWJ_C10 complex docking results show that ligand C10 strongly binds with essential protein site residues. Multiple robust hydrogen bonds exist between His405(B) and Val440(B) and Asn442 (B) as shown in the interaction diagram with strong bond lengths reaching 3.04–3.22 Å that stabilize the complex formation. The hydrophobic interaction forces between Leu348(B), Val402(B) and Ala439(B) strengthen drug binding and parallel π-π stacking resonance forces help orientate the ligand inside the pocket. The 3D representation reveals that C10 binds closely to the site while its structure fits optimally in the pocket because of its hydrophobic and polar environment. The ligand engages in numerous non-covalent interactions that result in its excellent docking score of −11.4 which exceeds all other examined candidates. The stability of binding interactions between C10 and the pocket indicates potential suitability of C10 as a drug candidate. The combination of strong binding interactions, optimal positioning, and high docking scores affirms the potential of C10 as an effective inhibitor. Additional experiments with in vitro assays need to validate computational results while optimizing the configurations of future candidate drugs Figure 6.

3.5.2. Molecular dynamic analysis

A 100 ns molecular dynamics simulation revealed the structural stability of protein-ligand complex through the RMSD plot. The protein (Cα) RMSD reaches 1.5 Å stability point which confirms structural stability. The ligand shows variable RMSD values throughout the measurement period since it maintains dynamic relationships with the binding site. The initial ligand stays unstable until 40 nanoseconds before entering a partial equilibrium phase that confirms pocket alterations occurred. RMSD fluctuations of the ligand suggest either changes in binding modes or brief protein-ligand interactions. Additional analyses including hydrogen bonding and MM-GBSA calculation are essential to validate the ligand's binding stability because of its observed dynamic nature. During molecular dynamics simulation the Root Mean Square Fluctuation (RMSF) plot reveals specific residue flexibility of the target protein. Most areas of the protein structure maintain stability through RMSF measurements which remain below 1.5 Å. The fluctuation range surpassing 2.5 Å is observed in specific regions

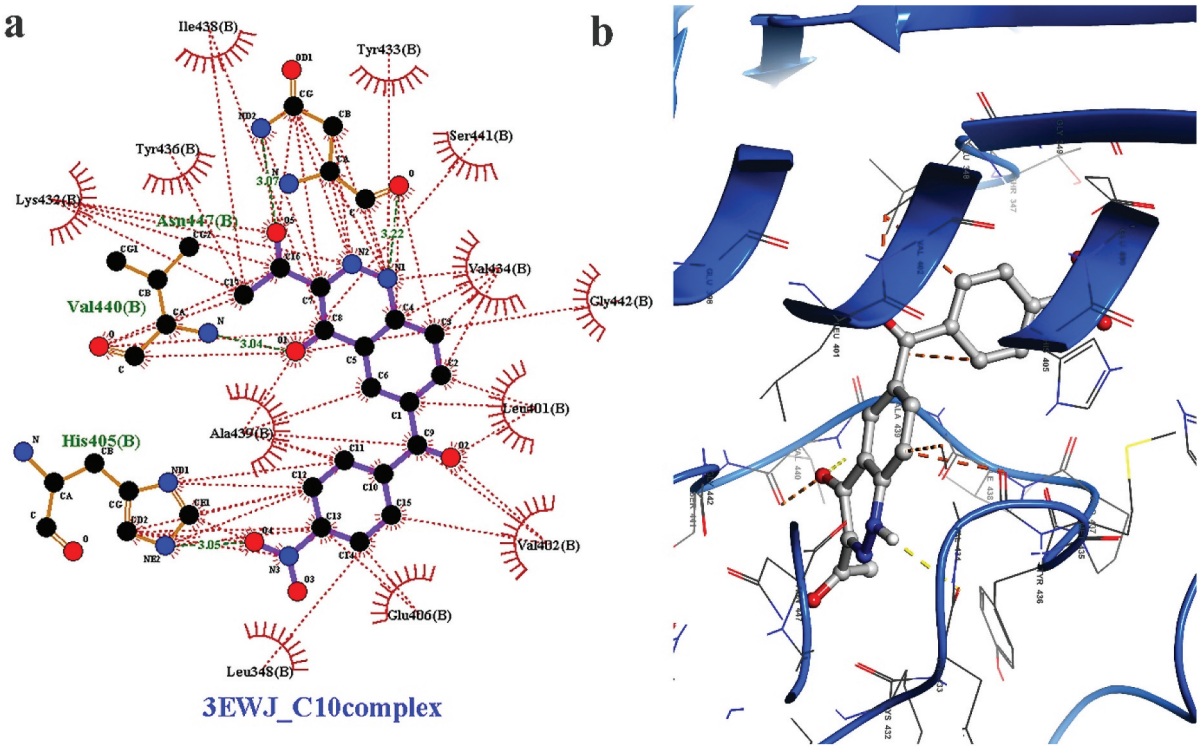

Figure 6. Molecular interactions of C10 within the 3EWJ active site: (a) 2D interaction map highlighting hydrogen bonds and hydrophobic contacts, (b) 3D visualization showing ligand binding and protein conformation.

which correspond to residues 180 through 220. These areas depict flexible loop regions along with terminal end structures. Green bars in the graph represent ligand-binding residues that demonstrate lower fluctuation patterns which indicate stable bonds between ligand and protein. The data indicates the binding area maintains high stability since other parts of the protein adapt to changes in shape. Studies of hydrogen bonds and secondary structure would provide solid evidence about how the ligand affects protein stability.

The MD simulations combined with docking analysis show essential protein-ligand binding interactions. The 2D plot reveals that hydrogen bonding exists between HIS 405 with an association of 55% and SER 441 at 62% and VAL 440 at 71% but also shows water-mediated bonding with GLU 398 at 45%. Laboratory tests show that the ligand molecule receives strong stabilizing binding from the active site. Results from the interaction histogram demonstrate forward and backward engagement of HIS 405, GLU 398, and SER 441 during the simulation period based on their interaction fractions surpassing 0.6. The changing contact patterns between ligand and protein demonstrate strong binding ability which needs additional free energy analysis to validate both pharmacological importance and binding stability. The 100 ns molecular dynamics simulation reveals information about long-lasting protein-ligand contacts through the protein-ligand contact timeline. The top plot presents the total interaction count which displays stable ligand binding through its movement between 5 and 15 contacts. Numerous contacts during simulations indicate that important binding residues include HIS 405, GLU 398, SER 441 and VAL 440 according to the lower heatmap Figure 7. The analysis shows that both GLU 402 and LYS 427 create brief yet forceful interactions with each other.

3.5.3. ADMET analysis

The compound C10 shows various desirable properties during its physicochemical analysis. The chemical compound exists in the drug-likeness range because it has a molecular weight of 337.29 g/mol. Membrane permeability and bioavailability can be expected from this compound because its total polar surface area (TPSA) reaches 125.71 $Å^2$. The LogP lipophilicity ratings between 1.50 and 3.61 indicate equal hydrophilic and lipophilic properties essential for absorption and distribution into the body. The compound exhibits

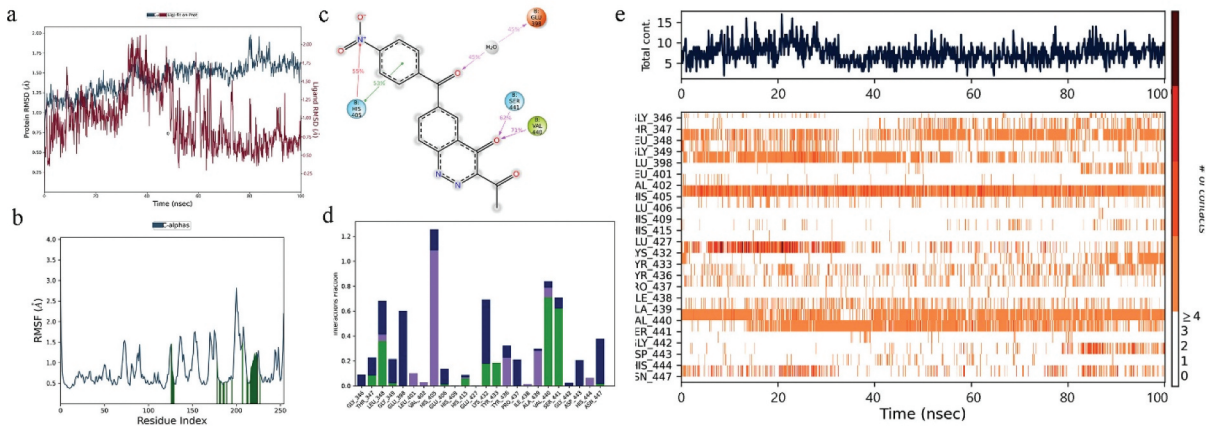

Figure 7. (a) RMSD plot of protein and ligand. (b) RMSF of protein residues. (c) 2D ligand interaction map. (d) Interaction frequency histogram. (e) Protein-ligand contact timeline.

hydrogen bond acceptor quantity of six along with 2 hydrogen bond donors that matches the Lipinski's rule of five requirements.

Data shows that this substance exists within the moderately soluble category with a Log S (ESOL) value set at −3.61. Scientific simulations show the substance absorbs well in the gastrointestinal tract but cannot pass through the blood-brain barrier thus decreasing the potential for central nervous system side effects. The compound demonstrates resistance to P-glycoprotein (Pgp) through its lack of substrate behavior.

The laboratory tests confirm that the compound blocks the metabolic functions of CYP2C19 and CYP2C9 so it affects how medicinal compounds interact within the body. This compound fails to inhibit CYP3A4 activity even though it shows inhibitory effects on CYP2C19 and CYP2C9 which decreases metabolic drug interactions.

The molecule follows most drug-likeness standards but features two PAINS alerts located on the nitro group and oxygen-nitrogen single-bond moiety. The synthetic accessibility scoring system shows that compound production will be straightforward with a score of 2.50. Research results should evaluate C10 due to its encouraging pharmacological potential and acceptable drug properties along with controlled drawbacks Figure 8.

3.5.4. Density functionality theory

The analysis of compound C10 electronic properties occurred through frontier molecular orbital (FMO) theory. Energy optimization calculations delivered HOMO energies of −8.65894 eV whereas LUMO

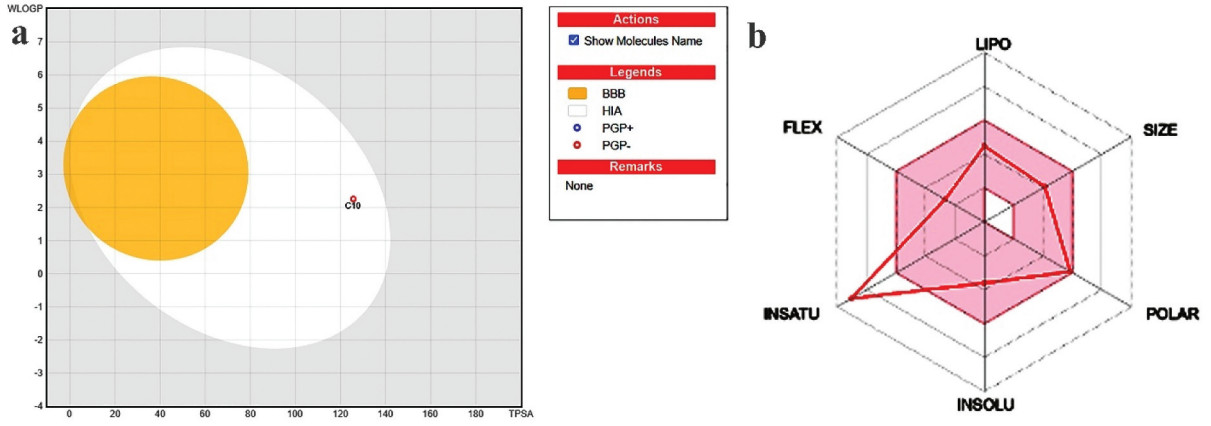

Figure 8. Physicochemical and pharmacokinetic profile of compound C10, showing balanced lipophilicity, moderate solubility, favorable absorption, and CYP450 interaction potential, with drug-likeness and synthetic accessibility properties highlighted.

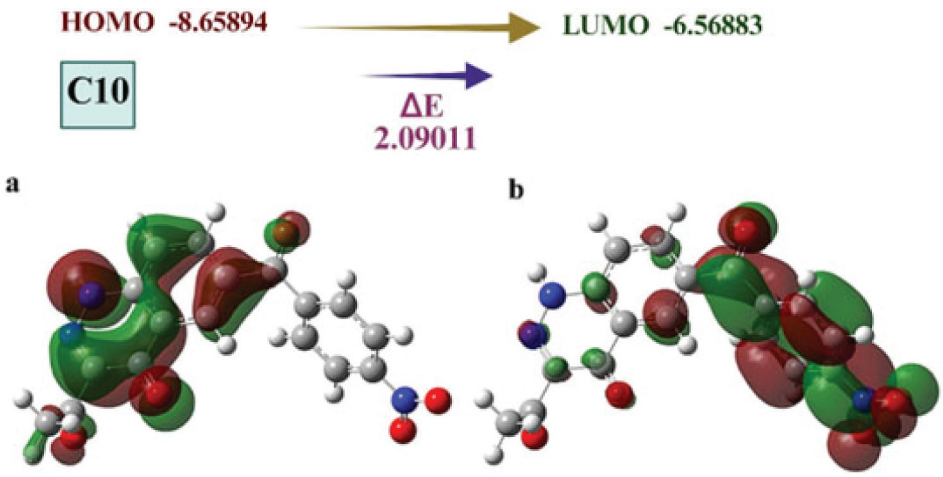

Figure 9. Frontier molecular orbitals of compound C10: (a) Highest Occupied Molecular Orbital (HOMO), showing electron density localization in donor regions, and (b) Lowest Unoccupied Molecular Orbital (LUMO), highlighting acceptor sites

energies amounted to −6.56883 eV. A moderate electronic stability with reactivity emerged from the HOMO-LUMO energy gap measurement which resulted in 2.09011 eV. The HOMO distribution displays electron density primarily situated near the aromatic structures and electron-donating functional groups since these areas perform key roles in charge donation throughout chemical reactions. Electrophilic attack occurs most favorably around the electron-withdrawing components in the LUMO space (**Figure 9**). The electrons distribution is reliant on the aromatic structure, and the electron-donating property is due to the acetyl group, which is located next to the cinnoline ring. The electron density in HOMO is largely localized to the aromatic structures, as well as the electron-donating functional groups. In detail, the LUMO is localized on nitrobenzoyl moiety of C10, which means that the nitro is an electron-withdrawing center and lowers the electron density of the LUMO. Meanwhile, the remaining part of the molecule particularly the cinnoline ring and the acetyl moiety also add to the HOMO and so contribute to the electronic properties of C10 in all its completeness which is imperative for its reactivity in biochemical applications. The electronic transition balance indicated by the medium HOMO-LUMO gap makes C10 suitable for optoelectronic usage or pharmaceutical scaffold development. The small HOMO-LUMO gap indicates the molecule has greater reactivity potential for biochemical applications.

3.6. Spectral data's

3.6.1. Ethyl 2-(2-(4-chlorophenyl) hydrazineylidene)-3-oxobutanoate (1I)

Yield (%): 82; m.p. (°C): 146-148. IR (cm^{-1}): 3316 (NH), 3009 (Ar-CH), 2932 (CH_2-CH), 1725 (C = O), 1658 (C = N), 1610 (C = C), 734 (C-Cl). ^{1}H-NMR (δ: ppm): 6.94-7.67 (4 H, m, Ar-CH), 6.41 (1H, s, NH), 2.95 (q, 2 H, CH_2), 2.38 (3 H, t, CH_3), 1.62 (3 H, s, $COCH_3$). ^{13}C-NMR (δ: ppm): 202.7 ($\underline{C}OC_2H_5$), 197.3 ($\underline{C}OCH_3$), 147.6 (C-1), 130.9 (N = C), 127.1 (C-3 & C-5), 121.9 (C-4), 114.5 (C-2 & C-6), 36.2 ($CO\underline{C}H_2$), 29.7 ($CO\underline{C}H_3$) , 21.0 (CH_3). MS (EI) m/z: 270 (M^{+2}), 268 (M^+). Anal. Calcd for $C_{12}H_{13}ClN_2O_3$: C, 53.64; H, 4.88; N, 10.43. Found: C, 53.79; H, 4.86; N, 10.40.

3.6.2. 3-acetyl-6-chlorocinnolin-4(1H)-one (2I)

Yield (%): 76; m.p. (°C): 252-255. IR (cm^{-1}): 3348 (NH), 3015 (Ar-CH), 2902 (CH_2-CH), 1746 (C = O), 1651 (C = N), 1609 (C = C), 714 (C-Cl). ^{1}H-NMR (δ: ppm): 6.70-7.26 (3 H, m, Ar-CH), 6.19 (1H, s, NH), 2.73 (3 H, s, $COCH_3$). ^{13}C-NMR (δ: ppm): 189.5 ($\underline{C}OCH_3$), 180.8 (C-4), 152.1 (C-3), 144.4 (C-9), 141.9 (C-7), 130.7 (C-10), 128.2 (C-5), 122.6 (C-6), 113.4 (C-8), 27.2 (CH_3). MS (EI) m/z: 224 (M^{+2}), 222 (M^+). Anal. Calcd for $C_{10}H_7ClN_2O_2$: C, 53.95; H, 3.17; N, 12.58. Found: C, 54.12; H, 3.18; N, 12.54.

3.6.3. 3-acetyl-6-(4-nitrobenzoyl)cinnolin-4(1H)-one (C10)

Yield (%): 79; m.p. (°C): 180-183. IR (cm^{-1}): 3291 (NH), 3024 (Ar-CH), 2920 (CH_2-CH), 1718 (C = O), 1643 (C = N), 1615 (C = C), 1548 & 1356 (NO_2). ^{1}H-NMR (δ: ppm): 6.87-7.91 (7 H, m, Ar-CH), 6.44 (1H, s, NH), 2.59 (3 H, s, $COCH_3$). ^{13}C-NMR (δ: ppm): 202.6 (CO), 197.2 ($\underline{C}OCH_3$), 174.7 (C-4), 159.5 (C-3), 155.1 (C'-4), 151.1 (C-9), 148.6 (C'-1), 135.4 (C-7), 134.9 (C'-2 & C'-6), 134.0 (C-5), 133.8 (C-6), 126.3 (C-10), 123.5 (C'-3 & C'-5), 119.5 (C-8), 21.5 (CH_3). MS (EI) m/z: 337 (M^+). Anal. Calcd for $C_{17}H_{11}N_3O_5$: C, 60.54; H, 3.29; N, 12.46. Found: C, 60.32; H, 3.30; N, 12.49.

3.6.4. Chemistry

In the present work, novel 3-acetyl-6-(substitute benzoyl)cinnolin-4(1H)-one (C1-C25) were prepared from 4-chloroaniline. In this synthesis, initially 4-chloroaniline undergoes diazotization reaction by reacting with sodium nitrite and hydrochloric acid and produces respective diazonium chloride analog. Later the formed diazonium chloride reacts with ethylacetoacetate in the presence of sodium acetate and produces ethyl 2-(2-(4-chlorophenyl) hydrazineylidene)-3-oxobutanoate (1I). In the next stage compound 1I undergoes ring closure reaction in the presence of aluminum chloride & chlorobenzene and produced 3-acetyl-6-chlorocinnolin-4(1H)-one (2I). Finally compound (2I) reacts with 4-nitrobenzaldehyde in the presence of sodium hydroxide & produced respective benzoyl derivatives i.e., 3-acetyl-6-(4-nitrobenzoyl)cinnolin-4(1H)-one (C10) through benzoylation reaction. Throughout the reactions, TLC was performed to optimize the completion of reactions & their purity.

The disappearance of absorption peak in IR around 750 cm^{-1} corresponds to C-Cl stretching, confirms the formation of 3-acetyl-6-(4-nitrobenzoyl) cinnolin-4(1H)-one (C10). This is further supported by the appearance of absorption peak in IR at 3291 cm^{-1}, 3024 cm^{-1}, 1718 cm^{-1}, & 1548 & 1356 cm^{-1} correspond to NH, Ar-CH, CH_2-CH, & NO_2 stretching, respectively. In addition, the appearance of the seven-proton multiplet in NMR at δ 6.87-7.91 ppm corresponds to aromatic proton, one proton singlet at δ 6.44 ppm corresponds to -NH- proton & three proton singlet at δ 2.59 ppm corresponds to $COCH_3$ proton further confirming the formation of compound C10. This is further supported by the appearance of absorption peak in ^{13}C-NMR around δ 202.6 ppm corresponds to C = O carbon. Additionally in IR, ^{1}H-NMR & ^{13}C-NMR spectroscopy emergence of various other peaks for assigned structures Figure I1, 2I and C10 confirms the chemical structure of target derivative C10. The molecular weight & purity of prepared analogs were confirmed from their mass spectrum.

3.6.5. Cytotoxicity analysis using MTT assay

Researchers evaluated the cell-killing capability of compound C10 through MTT testing against the MCF-7 breast cancer cells. An increasing amount of C10 within the solution leads to declining cell survival rates according to the study results Figure 10 and Table 1. The mean cell survival rate at 6.25 μg/mL reached 90.43% which shows that the compound is almost nontoxic to cells. The 12.5 μg/mL concentration of compound C10 resulted in a significant decrease in cell viability down to 77.32%. An increased compound C10 dosage from 25 μg/mL to 50 μg/mL and finally 100 μg/mL resulted in a stepwise reduction of cell viability to reach 60.32%, 41.95% and 33.82% respectively. Cells treated with 41.3 μg/mL C10 showed moderate cytotoxicity effects against MCF-7 cells according to the calculated IC_{50} value. Experimental results proved reliable based on the low standard deviation values between replicates which ranged from 0.10 to 1.33. Research indicates that C10 demonstrates dose-dependent destruction toward cancer cells which makes it a promising therapeutic option for treating breast cancers that express hormone receptors. Higher C10 concentration levels trigger substantial cell viability decreases indicating effective proliferation inhibition that might happen through apoptotic mechanisms or disrupted metabolic pathways. Next to other tested chemotherapeutic agents C10 shows moderate effectiveness through its IC_{50} value and this ability makes it worth developing into a more potent compound. Serving as a clear indicator for effective therapy when cancer cells receive selective treatment without causing significant damage to regular cells. Additional research is needed to explain how C10 functions by determining if it triggers apoptosis or stops the cell cycle.

The distinctive chemical makeup of cinnoline scaffolds makes them highly important for translational applications in pharmacological research. Their ability to respond with biological targets including enzymes also positions these molecules well for therapeutic development in oncology and infectious diseases together with neurological disorders. Research on preclinical tested

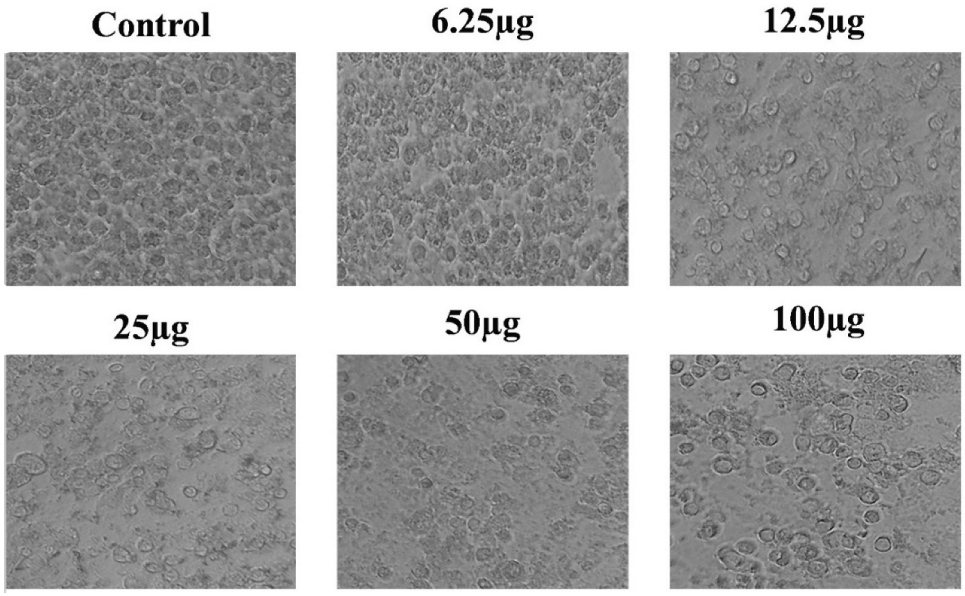

Figure 10. Microscopic images of MCF-7 cells treated with increasing concentrations of C10 (6.25–100 µg/mL), showing a dose-dependent reduction in cell density and morphological changes indicative of cytotoxicity.

Table 1. Dose-dependent cytotoxicity of compound C10 on MCF-7 cells. Microscopic observations at concentrations ranging from 6.25 to 100 µg/mL reveal reduced cell density and morphological alterations.

		OD at 570 nm			% Viability					
Sample	Concentration	Singlet	Duplicate	Triplicate	Singlet	Duplicate	Triplicate	Mean	SD	IC_{50} (µg)
Control	0	1.479	1.463	1.458	100	100	100	100		
C10	6.25	1.336	1.318	1.325	90.33130494	90.08885851	90.87791495	90.43269	0.4041808	41.3
	12.5	1.124	1.131	1.147	75.99729547	77.30690362	78.66941015	77.324536	1.3361446	
	25	0.892	0.884	0.878	60.31102096	60.42378674	60.21947874	60.318095	0.1023375	
	50	0.619	0.625	0.602	41.85260311	42.72043746	41.28943759	41.954159	0.7208851	
	100	0.497	0.506	0.485	33.60378634	34.58646617	33.26474623	33.818332	0.6864827	

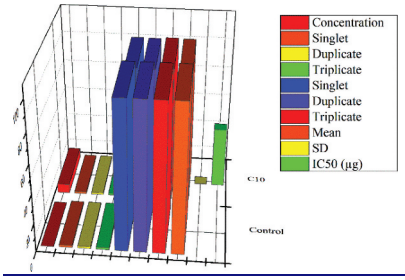

antimalarial and anticancer cinnoline derivatives supports their clinical development potential. Cinnoline scaffolds demonstrate their suitability for clinical improvements through adaptive target modification properties and good drug characteristics which enable future drug development for patient-oriented care.

The therapeutic potential of TACE (TNF-alpha converting enzyme) inhibitors has increased in cancer treatment since they interrupt tumor spread and inflammatory processes. The currently available TACE inhibitors TAPI-1 and TAPI-2 show promise because they restrict TACE enzymatic action to limit the release of pro-inflammatory cytokines TNF-α which subsequently reduces tumor spread and metastasis. There exists a limitation with these inhibitors because they fail to target TACE specifically leading to undesired effects. The binding affinity and high selectivity of cinnoline derivatives represented by C10 suggest these compounds offer enhanced treatment effect with fewer adverse effects when compared to established TACE inhibitors. Scientists continue investigating cinnoline derivatives because their selective properties make them strong candidates for cancer treatments by targeting the TACE enzyme to address earlier treatment challenges.

Acknowledgments

We have truly heartfelt gratitude to the management and administration of School of Pharmaceutical Sciences, Vels Institute of Science, Technology & Advanced Studies, Pallavaram, Chennai, Tamilnadu 600117, India for providing all the essential facilities that made this review article possible.

Saravanan Govindaraj, Panneerselvam Theivendren and Chidambaram Mylam Sreenivasan contributed to the conceptualization, methodology, software, validation, initial draft of the software writing, and the review and editing of the writing. All authors have reviewed and consented to the manuscript for submission.

Author contributions

CRediT: **Chidambaram Mylam Sreenivasan:** Conceptualization, Formal analysis, Investigation, Methodology, Validation, Writing – original draft; **Panneerselvam Theivendren:** Investigation, Methodology, Software, Writing – review & editing; **Saravanan Govindaraj:** Conceptualization, Investigation, Supervision, Validation, Writing – review & editing.

Disclosure statement

No potential conflict of interest was reported by the author(s).

ORCID

Panneerselvam Theivendren http://orcid.org/0000-0002-8197-4688
Saravanan Govindaraj http://orcid.org/0000-0002-1926-997X

References

[1] Arnold, M.; Morgan, E.; Rumgay, H.; Mafra, A.; Singh, D.; Laversanne, M.; Vignat, J.; Gralow, J. R.; Cardoso, F.; Siesling, S. Current and Future Burden of Breast Cancer: Global Statistics for 2020 and 2040. *Breast*. 2022, *66*, 15–23. DOI: 10.1016/j.breast.2022.08.010.

[2] W.H. Organization. Global Breast Cancer Initiative Implementation Framework: Assessing, Strengthening and Scaling-up of Services for the Early Detection and Management of Breast Cancer. World Health Organization. 2023.

[3] Chowdhury, A.; Kunjiappan, S.; Bhattacharjee, C.; Somasundaram, B.; Panneerselvam, T. Biogenic Synthesis of Marsilea Quadrifolia Gold Nanoparticles: A Study of Improved Glucose Utilization Efficiency on 3T3-L1 Adipocytes. *Vitro. Cell. Dev. Biol-Anim*. 2017, *53*(6), 483–493. DOI: 10.1007/s11626-017-0136-3.

[4] Theivendren, P.; Kunjiappan, S.; Hegde, Y. M.; Vellaichamy, S.; Gopal, M.; Dhramalingam, S. R.; Kumar, S. Importance of Protein Kinase and Its Inhibitor: A Review, Protein Kinases: Promising Targets for Anticancer Drug Research. *IntechOpen* 01. 2021, 75–100 doi:10.5772/intechopen.98552.

[5] Kunjiappan, S.; Panneerselvam, T.; Somasundaram, B.; Arunachalam, S.; Sankaranarayanan, M.; Parasuraman, P. Preparation of Liposomes Encapsulated Epirubicin-Gold Nanoparticles for Tumor Specific Delivery and Release. *Biomed. Phys. Eng. Express*. 2018, *4*(4), 45027. DOI: 10.1088/2057-1976/aac9ec.

[6] Coughlin, S. S.; Ekwueme, D. U. Breast Cancer as a Global Health Concern. *Cancer epidemiol*. 2009, *33*(5), 315–318. DOI: 10.1016/j.canep.2009.10.003.

[7] Becker, S. A Historic and Scientific Review of Breast Cancer: The Next Global Healthcare Challenge. *Int. J. Gynecol. Obstet*. 2015, *131*(S1), S36–S39. DOI: 10.1016/j.ijgo.2015.03.015.

[8] Pichaivel, M.; Anbumani, G.; Theivendren, P.; Gopal, M. An Overview of Brain Tumor. *Brain Tumors*. 2022, *1*, 1–10.

[9] Anderson, B. O.; Braun, S.; Carlson, R. W.; Gralow, J. R.; Lagios, M. D.; Lehman, C.; Schwartsmann, G.; Vargas, H. I. Overview of Breast Health Care Guidelines for Countries with Limited Resources. *Breast J*. 2003, *9*(s2), S42–S50. DOI: 10.1046/j.1524-4741.9.s2.3.x.

[10] Rose-John, S. ADAM17, Shedding, TACE as Therapeutic Targets. *Pharmacol. Res*. 2013, *71*, 19–22. DOI: 10.1016/j.phrs.2013.01.012.

[11] Rzymski, T.; Petry, A.; Kračun, D.; Riess, F.; Pike, L.; Harris, A.; Görlach, A. The Unfolded Protein Response Controls Induction and Activation of ADAM17/TACE by Severe Hypoxia and ER Stress. *Oncogene*. 2012, *31* (31), 3621–3634. DOI: 10.1038/onc.2011.522.

[12] Sen, P.; Kandasamy, T.; Ghosh, S. S. Multi-targeting TACE/ADAM17 and Gamma-Secretase of Notch Signalling Pathway in TNBC via Drug Repurposing Approach Using Lomitapide. *Cell. Signalling*. 2023, *102*, 110529. DOI: 10.1016/j.cellsig.2022.110529.

[13] Wang, S. E.; Xiang, B.; Guix, M.; Olivares, M. G.; Parker, J.; Chung, C. H.; Pandiella, A.; Arteaga, C. L. Transforming Growth Factor β Engages TACE and ErbB3 to Activate Phosphatidylinositol-3 Kinase/Akt in ErbB2-overexpressing Breast Cancer and Desensitizes Cells to Trastuzumab. *Mol. Cell. Biol.* 2008, *28*(18), 5605–5620. DOI: 10.1128/MCB.00787-08.

[14] Zhang, J.; Zhang, J.; Niu, X.; Zhou, Y.; Guo, Y.; Wang, Y.; Shou, F. Discussing the Safety and Effectiveness of Transcatheter Arterial Embolization Combined with Intravenous Chemotherapy in Treating Locally Advanced Breast Cancer. *Sci. Rep.* 2024, *14*(1), 6003. DOI: 10.1038/s41598-024-56642-w.

[15] Houthuijzen, J.; Jonkers, J. Cancer-associated Fibroblasts as Key Regulators of the Breast Cancer Tumor Microenvironment. *Cancer Metastasis Rev.* 2018, *37*(4), 577–597. DOI: 10.1007/s10555-018-9768-3.

[16] Narita, D.; Seclaman, E.; Ursoniu, S.; Anghel, A. Increased Expression of ADAM12 and ADAM17 Genes in Laser-Capture Microdissected Breast Cancers and Correlations with Clinical and Pathological Characteristics. *Acta Histochem.* 2012, *114*(2), 131–139. DOI: 10.1016/j.acthis.2011.03.009.

[17] Oh, K.; Lee, O.-Y.; Shon, S. Y.; Nam, O.; Ryu, P. M.; Seo, M. W.; Lee, D.-S. A Mutual Activation Loop between Breast Cancer Cells and Myeloid-Derived Suppressor Cells Facilitates Spontaneous Metastasis through IL-6 Trans-Signaling in A Murine Model. *Breast Cancer Res.* 2013, *15*(5), 1–16. DOI: 10.1186/bcr3473.

[18] Liu, X.; Deng, J.; Yuan, Y.; Chen, W.; Sun, W.; Wang, Y.; Huang, H.; Liang, B.; Ming, T.; Wen, J. Advances in Trop2-targeted Therapy: Novel Agents and Opportunities beyond Breast Cancer. *Pharmacol. Ther.* 2022, *239*, 108296. DOI: 10.1016/j.pharmthera.2022.108296.

[19] Selvam, T. P.; Karthick, V.; Kumar, P. V.; Ali, M. A. Synthesis and Structure-Activity Relationship Study of 2-(Substituted Benzylidene)-7-(4-Fluorophenyl)-5-(Furan-2-yl)-2H-Thiazolo [3, 2-a] Pyrimidin-3 (7h)-one Derivatives as Anticancer Agents. *Drug Discoveries Ther.* 2012, *6*(4), 198–204.

[20] Palanichamy, C.; Pavadai, P.; Panneerselvam, T.; Arunachalam, S.; Babkiewicz, E.; Ram Kumar Pandian, S.; Shanmugampillai Jeyarajaguru, K.; Nayak Ammunje, D.; Kannan, S.; Chandrasekaran, J. Aphrodisiac Performance of Bioactive Compounds from Mimosa Pudica Linn.: In Silico Molecular Docking and Dynamics Simulation Approach. *Molecules*. 2022, *27*(12), 3799. DOI: 10.3390/molecules27123799.

[21] Panneerselvam, T.; Kunjiappan, S.; Govindaraj, S.; Gopal, M.; Natarajan, K.; Hegde, Y. M.; Shanmugam, N.; Srinivas, G.; Ravi, K.; Natarajan, V. Graph Theoretical Analysis, in Silico Modeling and Molecular Dynamic Studies of (5-((2-Chloropyridin-4-yl) oxy)-3-Phenyl-1H-Pyrazol-1-yl)-2-(4-Substituted Phenyl)-N, N-Dimethylethen-1-Amine Derivatives for the Treatment of Breast Cancer. *Anti-Cancer Agents Med. Chem.* 2022, *23*. DOI: 10.2174/1871520623666221205140328.

[22] Mandhadi, J. R.; Panneerselvam, T.; Parasuraman, P. DESIGN, in Silico Modeling, Toxicity Study and Synthesis of Novel Substituted Semicarbazide Derivatives of Pyrimidine: An Antitubercular Agent. *Curr. Bioact. Compd.* 2020, *16*(3), 294–301. DOI: 10.2174/1573407214666181001112601.

[23] Rajeshkumar, R. R.; Kumar, B. K.; Parasuraman, P.; Panneerselvam, T.; Sundar, K.; Ammunje, D. N.; Pandian, S. R. K.; Murugesan, S.; Kabilan, S. J.; Kunjiappan, S. Graph Theoretical Network Analysis, in Silico Exploration, and Validation of Bioactive Compounds from *Cynodon Dactylon* as Potential Neuroprotective Agents against α-synuclein. *BioImpacts: BI*. 2022, *12*(6), 487. DOI: 10.34172/bi.2022.24113.

[24] Saravanan, G.; Panneerselvam, T.; Kunjiappan, S.; Parasuraman, P.; Alagarsamy, V.; Udayakumar, P.; Soundararajan, M.; Joshi, S. D.; Ramalingam, S.; Ammunje, D. N. Graph Theoretical Analysis, in Silico Modeling, Prediction of Toxicity, Metabolism and Synthesis of Novel 2-(Methyl/Phenyl)-3-(4-(5-Substituted-1, 3, 4-Oxadiazol-2-yl) Phenyl) Quinazolin-4 (3h)-ones as NMDA Receptor Inhibitor. *Drug Dev. Res.* 2019, *80*(3), 368–385. DOI: 10.1002/ddr.21511.

[25] Han, Z.; Song, L.; Qi, K.; Ding, Y.; Wei, M.; Jia, Y.; Zhang, Z. Deciphering the Key Pharmacological Pathways and Targets of Yisui Qinghuang Powder that Acts on Myelodysplastic Syndromes Using a Network Pharmacology-Based Strategy. *Evid.-Based Complementary Altern. Med.* 2020, *2020*(1), 8877295. DOI: 10.1155/2020/8877295.